



HAL
open science

**New standard magnetic field values determined by
cancellations of 85Rb and 87Rb atomic vapors $52\text{S}_{1/2} \rightarrow 62\text{P}_{1/2}, 3/2$ transitions**

Rodolphe Momier, Artur Aleksanyan, Emil Gazazyan, Aram Papoyan, Claude
Leroy

► **To cite this version:**

Rodolphe Momier, Artur Aleksanyan, Emil Gazazyan, Aram Papoyan, Claude Leroy. New standard magnetic field values determined by cancellations of 85Rb and 87Rb atomic vapors $52\text{S}_{1/2} \rightarrow 62\text{P}_{1/2}, 3/2$ transitions. *Journal of Quantitative Spectroscopy and Radiative Transfer*, 2020, 257, pp.107371. 10.1016/j.jqsrt.2020.107371 . hal-03365286

HAL Id: hal-03365286

<https://hal.science/hal-03365286>

Submitted on 17 Oct 2022

HAL is a multi-disciplinary open access archive for the deposit and dissemination of scientific research documents, whether they are published or not. The documents may come from teaching and research institutions in France or abroad, or from public or private research centers.

L'archive ouverte pluridisciplinaire **HAL**, est destinée au dépôt et à la diffusion de documents scientifiques de niveau recherche, publiés ou non, émanant des établissements d'enseignement et de recherche français ou étrangers, des laboratoires publics ou privés.



Distributed under a Creative Commons Attribution - NonCommercial 4.0 International License

New standard magnetic field values determined by
cancellations of ^{85}Rb and ^{87}Rb atomic vapors
 $5^2S_{1/2} \rightarrow 6^2P_{1/2, 3/2}$ transitions

Rodolphe MOMIER^a, Artur ALEKSANYAN^{a,b}, Emil GAZAZYAN^{b,c},
Aram PAPOYAN^b, Claude LEROY^{a,*}

^a*Laboratoire Interdisciplinaire Carnot de Bourgogne, UMR CNRS 6303, Université
Bourgogne Franche-Comté, 21000 Dijon, France*

^b*Institute for Physical Research, NAS of Armenia, Ashtarak-2, 0203 Armenia*

^c*Yerevan State University, Yerevan, 0025 Armenia*

Abstract

In this article, we study the theoretical behaviour of all the possible hyperfine transitions (π , σ^+ and σ^-) between the $5S$ and $6P$ states of ^{87}Rb and ^{85}Rb atomic vapors under the influence of an external magnetic field B . We show that, for specific transitions, we obtain one or several B -values for which the transition intensity is cancelled. The precision of these values is limited to the uncertainty of the physical quantities that are involved in the problem, thus measuring precisely the B -values for the cancellations could be a way to determine these quantities more precisely. In the simplest cases involving 2×2 hamiltonians, we give eigenvectors, eigenvalues and analytical formulas to determine the transition cancellation. By checking accuracy between formulas and numerical simulations, we conclude that it is possible to use the latter in order to determine all the cancellations even in the most complicated cases.

Keywords: Hyperfine structure, Zeeman effect, Polarization, Atomic spectroscopy

*Corresponding author: claude.leroy@u-bourgogne.fr

1. Introduction

Alkali have been deeply studied for several years mainly because of their one-electron structure in their valence shell. Spectroscopic data for these metals are well known [1]. Due to their simple energy-level structure, alkali are widely used to study Bose-Einstein condensates [2]. Moreover, alkali have transition frequencies ranging from near-infrared to mid-visible, thus is it possible to do experiments with cheap lasers. Alkali are also, for example, studied in magnetometry or information storage [3, 4]. When placed under the influence of an external magnetic field B , energy levels split into hyperfine sublevels (Zeeman effect) [5–7]. The hyperfine manifold of 5S and 6P states of both rubidium isotopes is presented on figure 1. The theoretical model to study transitions between these hyperfine sublevels has been developed in the 1990s by Tremblay *et al.* [8]. It is well known that in intermediate magnetic fields, the splitting of atomic energy levels into Zeeman sublevels deviates from the linear behavior, and the atomic transition probabilities undergo significant changes [8, 9]. To study such transitions, sub-Doppler methods have to be used because of Doppler broadening [10]. A lot of work has been performed concerning D_1 and D_2 lines and good results have been obtained using derivative selective reflection method [11–13].

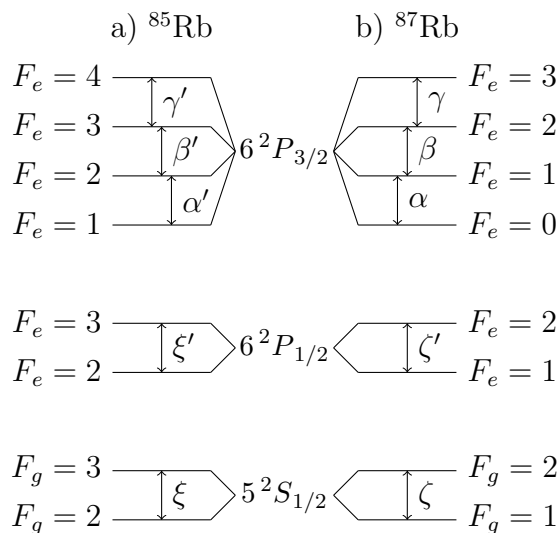


Figure 1: Hyperfine manifold of the 5S and 6P states of a) ^{85}Rb and b) ^{87}Rb . Figure not to scale. See table 1 for the splittings.

In this article, we study $5^2S_{1/2} \rightarrow 6^2P_{1/2, 3/2}$ transitions. Very little information on these transitions is available in the literature [14]. The energy level manifold is presented in figure 1 and hyperfine splittings (along with references) are provided in table 1. We will compute all the possible transitions between Zeeman sublevels and present a full formalism for the most simple cases ($5^2S_{1/2} \rightarrow 6^2P_{1/2}$ transitions) to determine transition cancellations. For the case $5^2S_{1/2} \rightarrow 6^2P_{3/2}$, we present numerical results.

Atom	State	Hyperfine splitting (MHz)	Reference
^{85}Rb	$5^2S_{1/2}$	$\xi = 3035.7324390(60)$	[15]
	$6^2P_{1/2}$	$\xi' = 117.33(66)$	[14]
	$6^2P_{3/2}$	$\alpha' = 9.802(25)$	
		$\beta' = 20.850(24)$	
		$\gamma' = 39.265(23)$	
^{87}Rb	$5^2S_{1/2}$	$\zeta = 6834.682610904290(90)$	[16]
	$6^2P_{1/2}$	$\zeta' = 265.12(66)$	[14]
	$6^2P_{3/2}$	$\alpha = 23.744(28)$	
		$\beta = 51.445(25)$	
		$\gamma = 87.050(23)$	

Table 1: Numerical values of the $5S$ and $6P$ hyperfine splittings.

2. Theoretical model

2.1. Hamiltonian of an atomic alkali vapor under the influence of an external magnetic field

The Hamiltonian \mathcal{H} of an atomic alkali vapor placed under the influence of an external static magnetic field B can be computed using the formalism presented in [8]. In the basis of the unperturbed atomic state vectors $|F, m_F\rangle$, matrix elements are given by

$$\langle F, m_F | \mathcal{H} | F, m_F \rangle = E_0(F) - \mu_B g_F m_F B \quad (1)$$

and

$$\begin{aligned}
\langle F-1, m_F | \mathcal{H} | F, m_F \rangle &= \langle F, m_F | \mathcal{H} | F-1, m_F \rangle \\
&= -\frac{\mu_B B}{2} (g_J - g_I) \left(\frac{[(J+I+1)^2 - F^2][F^2 - (J-I)^2]}{F} \right)^{1/2} \\
&\quad \times \left(\frac{F^2 - m_F^2}{F(2F+1)(2F-1)} \right)^{1/2}
\end{aligned} \tag{2}$$

where B is the projection of the magnetic field \vec{B} on the quantization axis. For the diagonal terms given by (1), $E_0(F)$ is the zero-field energy of the $|F, m_F\rangle$ sub-level, g_F is the associated Landé factor and m_F is the magnetic quantum number. It is important to note that the Bohr magneton has been chosen with a negative sign [1] so that the model remains consistent. The off-diagonal terms are given by (2), where g_J and g_I are respectively the total angular and nuclear Landé factors. These elements are non-zero only if they respect the selection rules $\Delta L = 0$, $\Delta J = 0$, $\Delta F = \pm 1$ and $\Delta m_F = 0$. A consequence of the two previous formula is that the Hamiltonian \mathcal{H} has a block diagonal structure where each block corresponds to a given value of m_F . This structure is similar to the one observed for the D_1 and D_2 lines of Rubidium [17]. In the case of $5^2S_{1/2} \rightarrow 6^2P_{1/2}$, blocks have a maximum size of 2×2 .

2.2. Transitions between two Zeeman sublevels

After diagonalization of the Hamiltonian, one obtains eigenvectors that can be expressed as linear combinations of the unperturbed atomic states vectors

$$|\Psi(F_g, m_{F_g})\rangle = \sum_{F'_g} c_{F_g F'_g} |F'_g, m_{F_g}\rangle \tag{3}$$

$$|\Psi(F_e, m_{F_e})\rangle = \sum_{F'_e} c_{F_e F'_e} |F'_e, m_{F_e}\rangle. \tag{4}$$

The calculation of the transition intensity A_{eg} between a "ground" Zeeman sublevel $|\Psi(F_g, m_{F_g})\rangle$ and an "excited" Zeeman sublevel $|\Psi(F_e, m_{F_e})\rangle$ is equivalent to the calculation of the squared transfer coefficients modified by the presence of the magnetic field B . These coefficients are given by the

following formula:

$$\begin{aligned}
& a[|\Psi(F_e, m_{F_e})\rangle; |\Psi(F_g, m_{F_g})\rangle; q] \\
& = \sum_{F'_e, F'_g} c_{F_e F'_e} a(F'_e, m_{F'_e}; F'_g, m_{F'_g}; q) c_{F_g F'_g}. \quad (5)
\end{aligned}$$

Equation (5) results in a sum of $n_g \times n_e$ terms (n_g and n_e being respectively the number of F_g and F_e levels) resulting in a combination of different magnetic quantum numbers. This combination can be cancelled as we will show later, which could be seen as quantum interferences.

The coefficients $a(F_e, m_{F_e}; F_g, m_{F_g}; q)$ are the unperturbed transfer coefficients given by

$$\begin{aligned}
& a(F_e, m_{F_e}; F_g, m_{F_g}; q) = (-1)^{1+I+J_e+F_e+F_g-m_{F_e}} \\
& \times \sqrt{2J_e+1} \sqrt{2F_e+1} \sqrt{2F_g+1} \begin{pmatrix} F_e & 1 & F_g \\ -m_{F_e} & q & m_{F_g} \end{pmatrix} \left\{ \begin{matrix} F_e & 1 & F_g \\ J_g & I & J_e \end{matrix} \right\} \quad (6)
\end{aligned}$$

where parenthesis represent a Wigner 3j-symbol and curly brackets represent a Wigner 6j-symbol. The index q depends on the polarization of the laser: $q = 0$ for π polarization and $q = \pm 1$ for σ^\pm polarization. In this article, we will denote the transitions as $|F_g, m_{F_g}\rangle \rightarrow |F_e, m_{F_e}\rangle$. Such transitions are allowed (resp. so-called forbidden) if they obey (resp. disobey) the selection rule $\Delta F = 0, \pm 1$. It is important to note that the notation $|F_g, m_{F_g}\rangle \rightarrow |F_e, m_{F_e}\rangle$ is an ambiguous notation since the application of a magnetic field causes a mixing of states, thus $|F, m_F\rangle$ is not a good basis in the meaning of eigenbases in intermediate magnetic fields, and neither is $|m_I, m_J\rangle$.

3. $5^2S_{1/2} \rightarrow 6^2P_{1/2}$ transitions

3.1. π transitions

On figures 2 and 3 are schematized all the possible $5^2S_{1/2} \rightarrow 6^2P_{1/2}$ π transitions of ^{87}Rb and ^{85}Rb . In this case, there are no forbidden transitions.

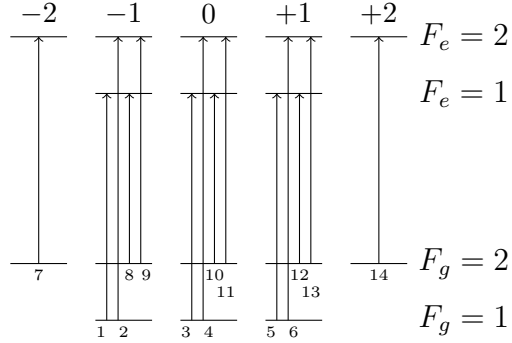


Figure 2: Possible $5^2S_{1/2} \rightarrow 6^2P_{1/2}$ π transitions of ^{87}Rb .

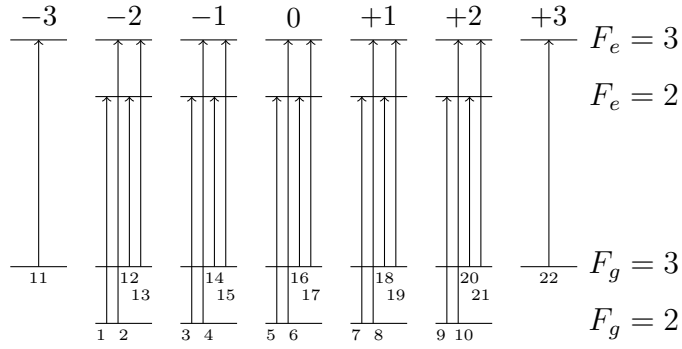


Figure 3: Possible $5^2S_{1/2} \rightarrow 6^2P_{1/2}$ π transitions of ^{85}Rb .

Using numerical simulations of the theoretical model described before, we can compute all the modified transfer coefficients $a[|\Psi(F_e, m_{F_e})\rangle; |\Psi(F_g, m_{F_g})\rangle; q]$ corresponding to these transitions. The results are shown on figures 4 and 5 for both isotopes.

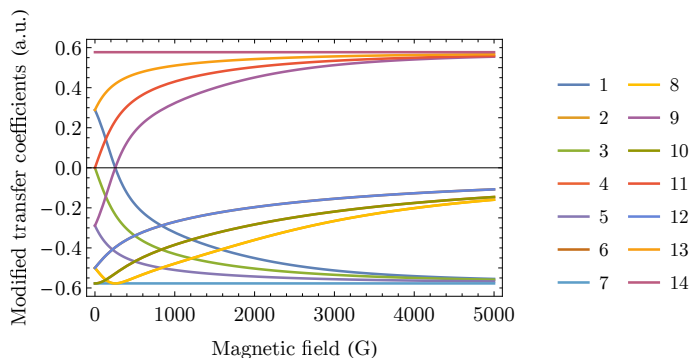


Figure 4: $5^2S_{1/2} \rightarrow 6^2P_{1/2}$ π transition modified transfer coefficients of ^{87}Rb .

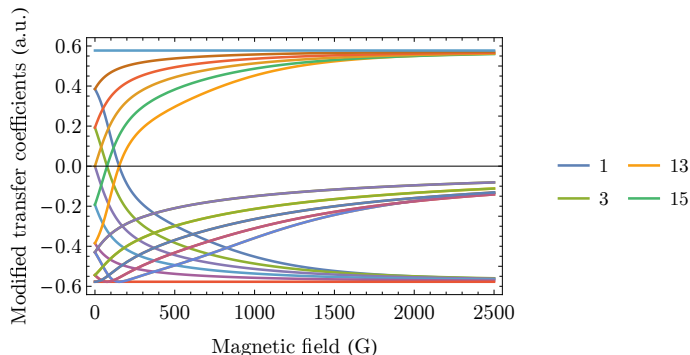


Figure 5: $5^2S_{1/2} \rightarrow 6^2P_{1/2}$ π transition modified transfer coefficients of ^{85}Rb . For the sake of clarity, only the coefficients with a cancellation are labelled.

We will first focus on ^{87}Rb . On figure 4 we notice that only two transfer coefficients cross the x -axis, meaning they are the only ones to cancel for a specific value of the external magnetic field B . These transfer coefficients correspond to the transitions labelled 1 and 9 (respectively $|F_g = 1, m_{F_g} = -1\rangle \rightarrow |F_e = 1, m_{F_e} = -1\rangle$ and $|F_g = 2, m_{F_g} = -1\rangle \rightarrow |F_e = 2, m_{F_e} = -1\rangle$). It is important to keep in mind that this notation is not the best as $|F, m_F\rangle$ is not a good basis in intermediate magnetic fields, although since the hyperfine sublevels are smoothly connected to the zero-field states, this notation still keeps a relevant meaning. The transfer coefficients have been computed using the following numerical data: $g_s = 2.00231930436256(35)$ [16], $\mu_B = -1.39962449361(42)$ MHz/G [18], $g_I = -0.0009951414(10)$ and $g_L = 0.99999369$ [1], and the splittings displayed in table 1. Note that, on

figure 4, we can see constant lines corresponding to the transitions labelled 7 ($|F_g = 2, m_{F_g} = -2\rangle \rightarrow |F_e = 2, m_{F_e} = -2\rangle$) and 14 ($|F_g = 2, m_{F_g} = +2\rangle \rightarrow |F_e = 2, m_{F_e} = +2\rangle$). This is simply due to the fact that they correspond to transitions to states that remain pure (non-mixed) and do not depend on the value of B . Since we are interested in transition cancellations, we will now focus on the states corresponding to $m_{F_g} = m_{F_e} = -1$ and derive analytical formulas. We do not need to compute the total Hamiltonian, it is sufficient to compute the two 2×2 blocks corresponding to the ground and excited states that we study. Using (1) and (2), we obtain

$$G = \begin{pmatrix} \mu_B B(2g_I - g_g) & \sqrt{3}\mu_B B(g_I - g_g) \\ \sqrt{3}\mu_B B(g_I - g_g) & \mu_B g_g B + \zeta \end{pmatrix} \quad (7)$$

$$E = \begin{pmatrix} \mu_B B(2g_I - g_e) & \sqrt{3}\mu_B B(g_I - g_e) \\ \sqrt{3}\mu_B B(g_I - g_e) & \mu_B g_e B + \zeta' \end{pmatrix} \quad (8)$$

where we denoted $g_g = \frac{3g_I}{4} + \frac{g_s}{4}$ and $g_e = \frac{3g_I}{4} + \frac{g_L}{3} - \frac{g_s}{12}$. The matrices G and E are written in the basis $|F, m_F\rangle$. After diagonalization, we obtain the following eigenvalues:

$$\lambda_{g\pm} = \frac{\zeta + 2\mu_B B g_I \pm [(\zeta + 2\mu_B B(g_g - g_I))^2 + 12\mu_B(g_g - g_I)B^2]^{\frac{1}{2}}}{2}$$

$$\lambda_{e\pm} = \frac{\zeta' + 2\mu_B B g_I \pm [(\zeta + 2\mu_B B(g_e - g_I))^2 + 12\mu_B(g_e - g_I)B^2]^{\frac{1}{2}}}{2}$$

where $\lambda_{g\pm}$ are the two eigenvalues of G and $\lambda_{e\pm}$ are the two eigenvalues of E . The eigenvectors can be decomposed on the basis of the unperturbed atomic state vectors according to (3) and (4). In this case, we obtain:

$$|\Psi(F_g, m_{F_g})\pm\rangle = \frac{\eta_{g\pm}}{\sqrt{1 + \eta_{g\pm}^2}} |1, -1\rangle + \frac{1}{\sqrt{1 + \eta_{g\pm}^2}} |2, -1\rangle \quad (9)$$

$$|\Psi(F_e, m_{F_e})\pm\rangle = \frac{\eta_{e\pm}}{\sqrt{1 + \eta_{e\pm}^2}} |1, -1\rangle + \frac{1}{\sqrt{1 + \eta_{e\pm}^2}} |2, -1\rangle \quad (10)$$

where we denoted

$$\eta_{g\pm} = \frac{\lambda_{g\pm} - \zeta - \mu_B g_g B}{\sqrt{3}\mu_B B(g_I - g_g)}$$

$$\eta_{e\pm} = \frac{\lambda_{e\pm} - \zeta' - \mu_B g_e B}{\sqrt{3}\mu_B B(g_I - g_e)}.$$

Making use of (5), we can write the modified transfer coefficients as

$$a[|\Psi(F_e, m_{F_e})\pm\rangle; |\Psi(F_g, m_{F_g})\pm\rangle; q = 0] \\ = \left[\sqrt{3}(\eta_{g\pm}\eta_{e\pm} - 1) + 3(\eta_{g\pm} + \eta_{e\pm}) \right] \frac{1}{6\sqrt{1 + \eta_{g\pm}^2}\sqrt{1 + \eta_{e\pm}^2}}.$$

These two transfer coefficients get cancelled for the same value of B as shown by the numerical simulation. We can determine that the B -value causing the transfer coefficients to be cancelled are given by:

$$B_{(\pm)}^{(\pm)} = \frac{1}{\mu_B} \frac{3\zeta\zeta'}{3g_I\zeta - 4g_L\zeta + g_s\zeta + 3g_I\zeta' - 3g_s\zeta'}. \quad (11)$$

This formula is analogous to the one determined by Aleksanyan *et al.* [19] for the D_1 line of ^{87}Rb . In table 2 we present the B -value obtained for both transitions using relation (11), where B is the value with its uncertainty and B^* is the value obtained when ignoring the uncertainty of the excited states' energy difference (ESED) ζ' . We notice that the major loss of precision on B comes from the small number of digits of ζ' . In this case, the numerical simulation provides a value of $B = 254.423942950$ G (all uncertainties ignored) which appears to be in perfect agreement with the formula we have derived (11). When recording the reflection or absorption spectra of an atomic vapor confined in a nano-cell, it is possible to measure the intensity of a transition and thus determine precisely the value of the external magnetic field when this transition cancels. This method would be even more efficient if an experiment was done to refine the value of ζ' . Consequently, such values can be implemented as a standard for precise magnetometers. Also on figures 4 and 5, one sees cancellations of transitions for $B = 0$, but in that case the Zeeman splitting does not exist and all the levels are degenerated. However, in order to null a magnetic field, it is preferable to use compensation measurement principle, as well explained in [20, 21].

Atom	Transitions	B (G)	B^* (G)
^{87}Rb	1	254.39(57)	254.398160387(80)
	9		

Table 2: B -values cancelling $^{87}\text{Rb } 5^2S_{1/2} \rightarrow 6^2P_{1/2} \pi$ transitions.

Analogously, on figure 5 we see that four transfer coefficients cross the x -axis. These coefficients correspond to the transitions labelled 1, 3, 13 and 15

(respectively $|F_g = 2, m_{F_g} = -2\rangle \rightarrow |F_e = 2, m_{F_e} = -2\rangle$, $|F_g = 2, m_{F_g} = -1\rangle \rightarrow |F_e = 2, m_{F_e} = -1\rangle$, $|F_g = 3, m_{F_g} = -2\rangle \rightarrow |F_e = 3, m_{F_e} = -2\rangle$ and $|F_g = 3, m_{F_g} = -1\rangle \rightarrow |F_e = 3, m_{F_e} = -1\rangle$). With the same type of calculations as before, focusing only on the blocks corresponding to $m_{F_g} = m_{F_e} = \pm 1$ and $m_{F_g} = m_{F_e} = \pm 2$, we obtain that the modified transfer coefficients mentioned before cancel for:

$$B_{(\pm)}^{(\pm)} = \frac{1}{\mu_B} \frac{2\xi\xi'}{3g_I\xi' - 3g_s\xi' + 3g_I\xi - 4g_L\xi + g_s\xi} \text{ for } m = -1 \quad (12)$$

$$B_{(\pm)}^{(\pm)} = \frac{1}{\mu_B} \frac{4\xi\xi'}{3g_I\xi' - 3g_s\xi' + 3g_I\xi - 4g_L\xi + g_s\xi} \text{ for } m = -2. \quad (13)$$

The results obtained are shown in table 3

Atom	Transitions	$B(\text{G})$	$B^*(\text{G})$
^{85}Rb	1	150.31(76)	150.31738954(20)
	13		
	3	75.15(38)	75.15869477(10)
	15		

Table 3: B -values cancelling $^{85}\text{Rb } 5^2S_{1/2} \rightarrow 6^2P_{1/2} \pi$ transitions

As before, two different types of B -values are shown. B is the value taking into account all the uncertainties and B^* is the value obtained when ignoring the uncertainty on the ESED ξ' . Both B and B^* are obtained using (12) and (13). Once again, we see that the numerical simulation and the theory are in perfect agreement (the values obtained numerically are $B = 75.15869477 \text{ G}$ for $m = -1$ and $B = 150.31738954 \text{ G}$ for $m = -2$). Consequently, we can use the numerical simulation to determine precisely the cancellations of transitions for which the calculations are heavier (when blocks are of size 3×3 or higher, as it happens for $6^2P_{3/2}$ states).

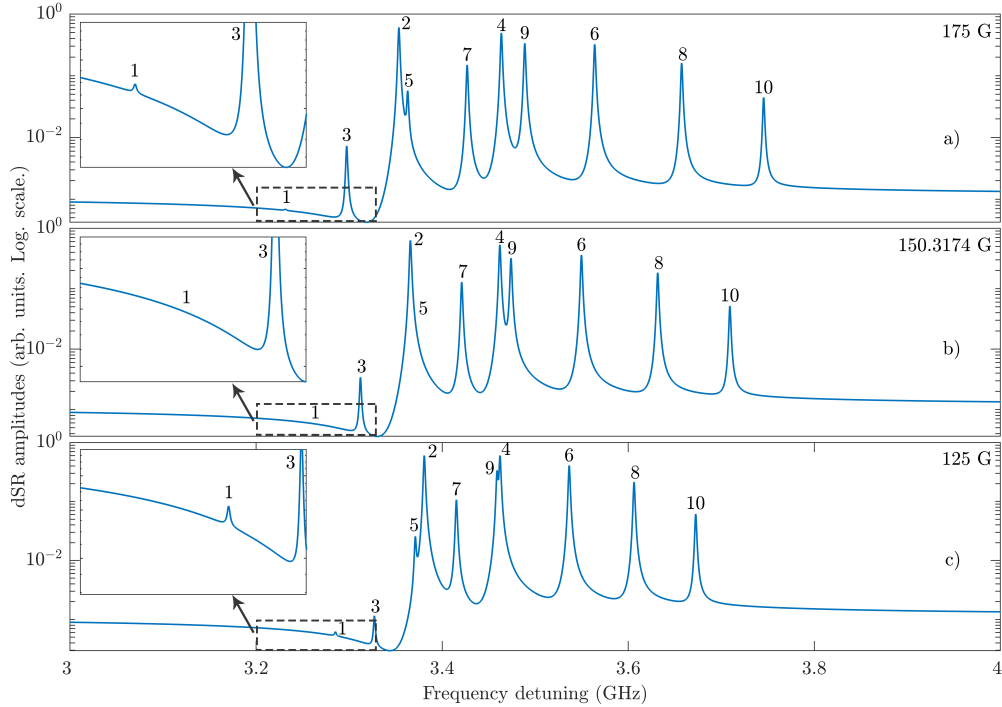


Figure 6: $^{85}\text{Rb } 5^2S_{1/2} \rightarrow 6^2P_{1/2}$ π -transitions spectra in magnetic field. a) $B = 175$ G, b) $B = 150.31739$ G, c) $B = 125$ G. Atomic density = 10^{13} cm^{-3} , laser power = 0.1 mW, $\lambda_{\text{laser}} = 780$ nm, $l = 380$ nm, temperature = 130 $^{\circ}\text{C}$.

On figure 6, as an illustration of our calculations we have computed one spectrum for the value $B = 150.31739$ G that cancels the transition $|F_g = 2, m_{F_g} = -2\rangle \rightarrow |F_e = 2, m_{F_e} = -2\rangle$, labelled 1 on figure 3 and table 3, and two other spectra for the values $B = 125$ G and $B = 175$ G. These spectra have been obtained by simulating a derivative selective reflection (dSR) experiment performed with a cell of length $l = 380$ nm at the temperature of 130 $^{\circ}\text{C}$. More detailed explanations and relations used to obtain these spectra can be found in [22]. It is worth to mention that these spectra indicate clearly the probable experimental difficulty to determine the B -values which cancel the transitions considered in the paper.

Before looking at the case of $5^2S_{1/2} \rightarrow 6^2P_{3/2}$ transitions, we will just present graphs of the σ^{\pm} transition intensities of both Rubidium isotopes.

3.2. σ^\pm transitions

On figures 7 and 8 are shown all the σ transition intensities between $5^2S_{1/2}$ and $6^2P_{1/2}$ states of ^{87}Rb and ^{85}Rb .

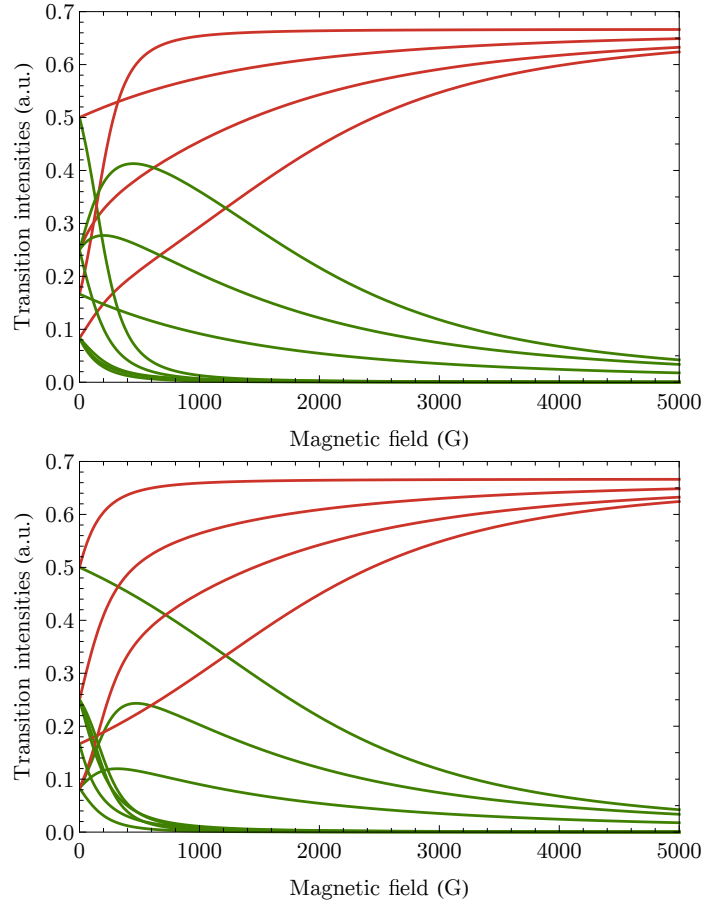


Figure 7: $^{87}\text{Rb } 5^2S_{1/2} \rightarrow 6^2P_{1/2}$ σ^+ (top) and σ^- (bottom) transition intensities.

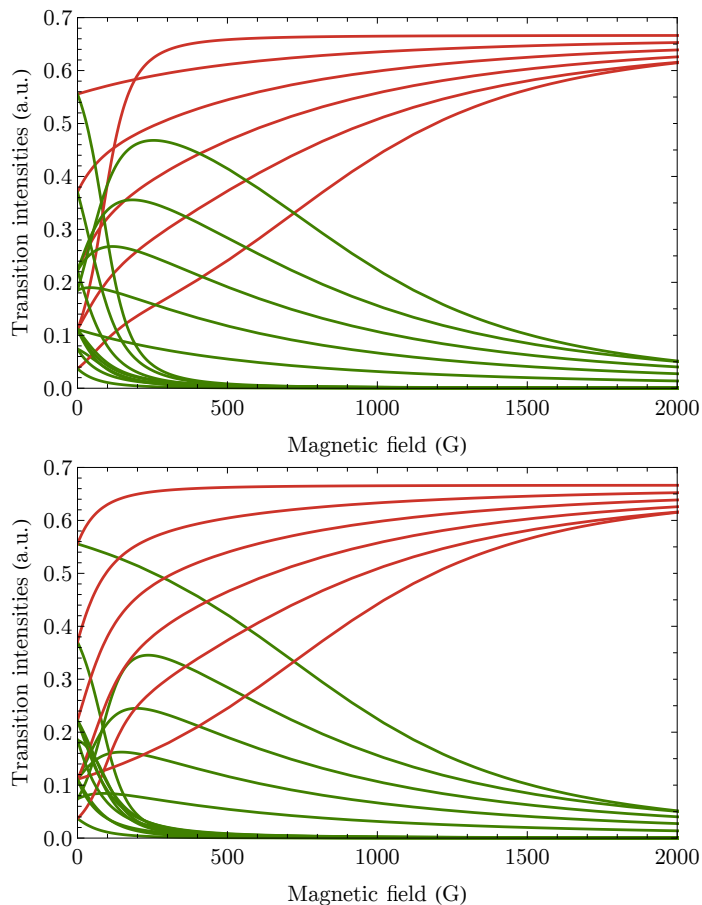


Figure 8: $^{85}\text{Rb } 5^2S_{1/2} \rightarrow 6^2P_{1/2} \sigma^+$ (top) and σ^- (bottom) transition intensities.

Transitions that remain present in the spectra at high magnetic fields are represented in red and the ones that vanish are represented in green. For these transitions, we do not provide labelling since they are not interesting for our study. Indeed, none of these transition intensities are cancelled for specific values of B .

To sum up, 38 different transitions are possible for ^{87}Rb (resp. 62 for ^{85}Rb). Among all these transitions, only 2 (resp. 4) get cancelled for specific values of B , all these transitions corresponding to a π polarization of the laser. Knowing that the numerical simulation is in full agreement with the theory, we will now use it to determine precisely cancellation of $5^2S_{1/2} \rightarrow 6^2P_{3/2}$ transitions for both isotopes.

4. $5^2S_{1/2} \rightarrow 6^2P_{3/2}$ transitions of rubidium 87

In this section, we will compute all the transition intensities of the possible π and σ^\pm transitions between $5^2S_{1/2}$ and $6^2P_{3/2}$. We will show graphs for the π and σ^\pm transitions of ^{87}Rb . Due to the complexity of the calculations, we will not derive analytical formulas since cancelled transitions involve 3×3 or 4×4 blocks.

4.1. π transitions

All the modified transfer coefficients corresponding to the transitions labelled on figure 9 are represented on figure 10. In this case, transitions 3, 7, 10 and 16 are forbidden in the general case but none of them cross the x -axis.

On this figure, all the curves vary according to the magnetic field since none of them correspond to transitions between two pure states. Among the 24 possible transitions, the transitions labelled 6, 9, 14, 17 and 20 have a cancellation. These transitions have a magnetic quantum number of either -1 , 0 or 1 , unlike for $5^2S_{1/2} \rightarrow 6^2P_{1/2}$ transitions where we only had $m = -1$ for ^{87}Rb . Here, each transition is cancelled for a different value of B . However, experimental measurements could be more difficult in this case due to the proximity of certain values.

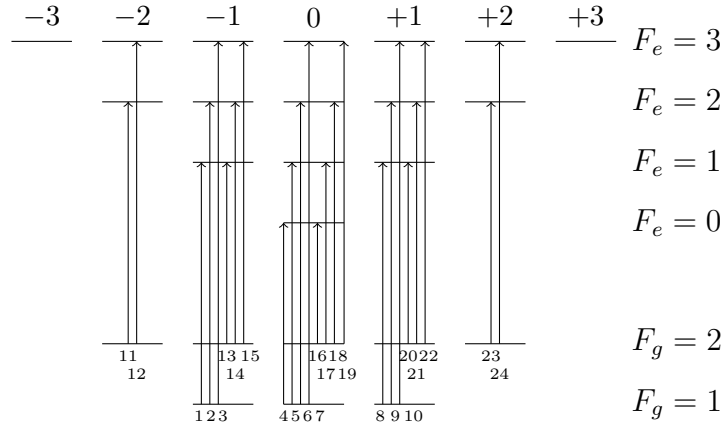


Figure 9: Possible $5^2S_{1/2} \rightarrow 6^2P_{3/2}$ π transitions of ^{87}Rb .

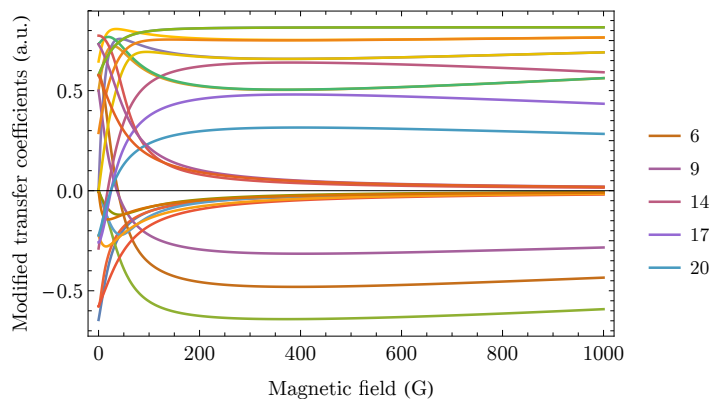


Figure 10: $5^2S_{1/2} \rightarrow 6^2P_{3/2}$ π transition modified transfer coefficients. For the sake of clarity, only the ones with a cancellation are labelled.

Table 4 shows the B -values for each cancellation, determined numerically with (3rd column) and without (4th column) taking into account the uncertainty on the ESEDs.

Atom	Transitions	B (G)	B^* (G)
^{87}Rb	6	38.152(19)	38.152597093(12)
	9	36.224(15)	36.224262166(11)
	14	17.8789(60)	17.8789466978(55)
	17	24.724(13)	24.7247536874(76)
	20	24.289(11)	24.2896121953(75)

Table 4: B -values cancelling ^{87}Rb $5^2S_{1/2} \rightarrow 6^2P_{3/2}$ π transitions.

4.2. σ^+ transitions

All the modified transfer coefficients corresponding to the transitions labelled on figures 11 and 12 are represented on figure 13.

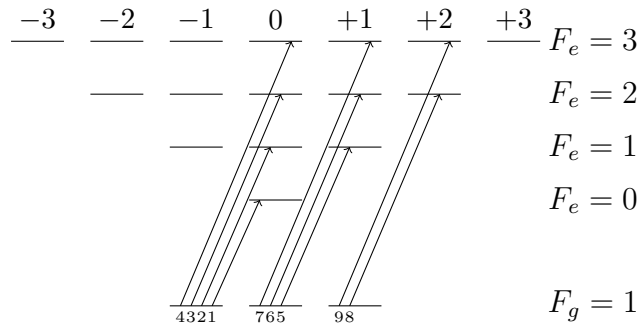


Figure 11: Possible $5^2S_{1/2} \rightarrow 6^2P_{3/2} \sigma^+$ transitions of ^{87}Rb , $F_g = 1$.

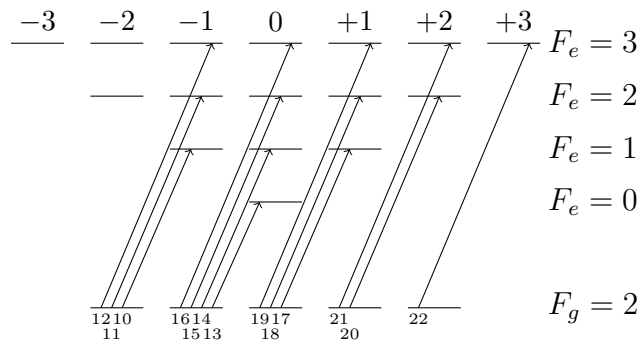


Figure 12: Possible $5^2S_{1/2} \rightarrow 6^2P_{3/2} \sigma^+$ transitions of ^{87}Rb , $F_g = 2$.

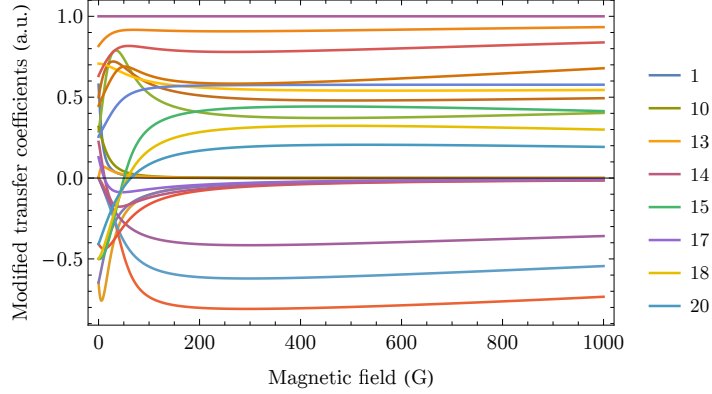


Figure 13: $5^2S_{1/2} \rightarrow 6^2P_{3/2} \sigma^+$ modified transfer coefficients. For the sake of clarity, only the ones with a cancellation are labelled.

Eight σ^+ transitions (respectively labelled 1, 10, 13, 14, 15, 17, 18 and 20, according to figures 11 and 12) are cancelled for a certain value of B . Transition 13 is a forbidden transition. The B -values are presented in table 5. Note the important number of cancellations compared to the case of $5^2S_{1/2} \rightarrow 6^2P_{1/2}$ where no cancellation could be observed for σ^\pm . We notice that the three B -values of transitions 1, 10 and 13 have much bigger uncertainties than the others.

For transition 20, we were able to exhibit the following analytical formula (among all these transitions it is the only one where Hamiltonians are of maximum 2×2 dimension):

$$B = -\frac{1}{\mu_B} \frac{4\gamma\zeta(3g_I(\gamma - \zeta) + 2\zeta g_L + g_S(\zeta - 3\gamma))}{c_1 c_2} \quad (14)$$

where we denoted $c_1 = 6\gamma g_I - 3\zeta g_I + 2\zeta g_L - 6\gamma g_S + \zeta g_S$ and $c_2 = 2\gamma g_I - 3\zeta g_I + 2\zeta g_L - 2\gamma g_S + \zeta g_S$. This formula provides a B -value for the cancellation $B = 64.164811472$ G (all uncertainties ignored) showing the theory to be in perfect agreement with the simulation.

Atom	Transitions	$B(\text{G})$	$B^*(\text{G})$
^{87}Rb	1	528(8)	528.89107942(16)
	10	606(4)	606.26243494(19)
	13	581(4)	581.79032289(18)
	14	12.1773(77)	12.1773749366(36)
	15	50.263(19)	50.263197219(15)
	17	11.2105(63)	11.2105200388(35)
	18	57.089(18)	57.089445775(18)
	20	64.164(18)	64.164811472(20)

Table 5: B -values cancelling $^{87}\text{Rb } 5^2S_{1/2} \rightarrow 6^2P_{3/2} \sigma^+$ transitions.

4.3. σ^- transitions

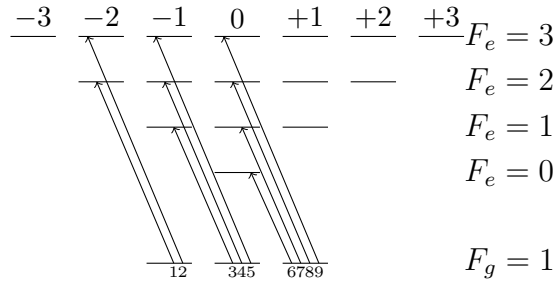


Figure 14: Possible $5^2S_{1/2} \rightarrow 6^2P_{3/2} \sigma^-$ transitions of ^{87}Rb , $F_g = 1$.

We schematize the possible σ^- transitions on figure 14 and 15. As for the σ^+ case, 22 transitions are possible in total. The modified transfer coefficients corresponding to all these transitions are represented on figure 16. Since cancelled transitions involve 3×3 or 4×4 blocks, we do not derive any analytical formula although it should be possible based on Ferrari and Cardano's formulas.

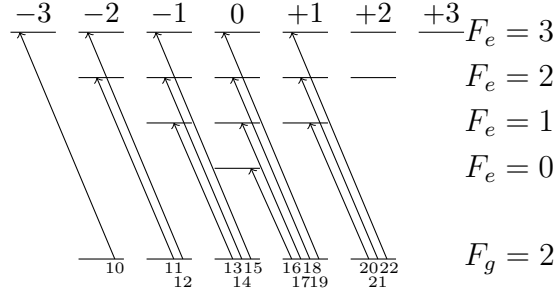


Figure 15: Possible $5^2S_{1/2} \rightarrow 6^2P_{3/2} \sigma^-$ transitions of ^{87}Rb , $F_g = 2$.

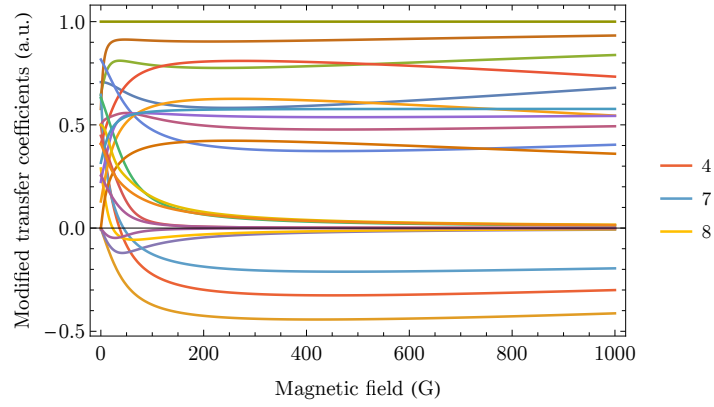


Figure 16: $5^2S_{1/2} \rightarrow 6^2P_{3/2} \sigma^-$ modified transfer coefficients. For the sake of clarity, only the ones with a cancellation are labelled.

Atom	Transitions	$B(\text{G})$	$B^*(\text{G})$
^{87}Rb	4	36.226(15)	36.226299830(11)
	7	44.053(32)	44.053383584(14)
	8	22.932(18)	22.9322893243(71)

Table 6: B -values cancelling $^{87}\text{Rb} 5^2S_{1/2} \rightarrow 6^2P_{3/2} \sigma^-$ transitions.

Again, as on figure 13, we observe a constant horizontal line corresponding to transition 10 which is a transition between pure states ($m_{F_g} = -2 \rightarrow m_{F_e} = -3$). Among the other curves, three get cancelled (transitions 4, 7 and 8, corresponding to respectively $m_{F_g} = 0, +1, +1$) for

precise values of B . Unlike before, no transition starting from $F_g = 2$ is cancelled. We will now present numerical data obtained for the all $5^2S_{1/2} \rightarrow 6^2P_{3/2}$ transition of ^{85}Rb .

5. $5^2S_{1/2} \rightarrow 6^2P_{3/2}$ transitions of rubidium 85

Hereafter we present all the $5^2S_{1/2} \rightarrow 6^2P_{3/2}$ transitions of rubidium 85 which show a cancellation and their associated B -values. In this case, 116 transitions are possible in total, thus, for the sake of clarity, we will not include graphical representations.

F_g	F_e	m_{F_g}	$B(\text{G})$	$B^*(\text{G})$
2	3	2	8.769(18)	8.7690392145(69)
2	3	1	9.459(16)	9.45921227700(74)
2	3	0	10.383(14)	10.3833071342(80)
2	3	-1	14.939(14)	14.939707247(12)
2	2	0	16.100(22)	16.100382502(13)
2	2	1	16.511(27)	16.511161122(13)
2	2	2	16.582(32)	16.582004270(14)
2	3	2	3968(20)	3968.442808(10)
2	3	1	4308(19)	4308.0783929(12)
2	3	0	4661(22)	4661.474736(12)
2	4	-1	5028(24)	5028.533960(13)

Table 7: B -values cancelling $^{85}\text{Rb } 5^2S_{1/2} \rightarrow 6^2P_{3/2} \sigma^-$ transitions.

F_g	F_e	m_{F_g}	$B(\text{G})$	$B^*(\text{G})$
2	2	-1	2.1781(46)	2.1781258679(16)
3	3	-1	4.1561(37)	4.1561596068(32)
3	3	-2	10.3069(82)	10.3069257317(79)
3	2	2	10.909(12)	10.9098105059(87)
3	2	1	11.089(13)	11.08932124359(87)
3	2	0	11.268(14)	11.2682145868(88)
3	2	-1	11.353(14)	11.3538322950(87)
2	3	-2	14.269(15)	14.269650745(11)
2	3	1	14.769(16)	14.796304738(12)
2	3	0	15.296(17)	15.296627412(12)
2	3	-1	15.733(18)	15.733434029(12)
2	4	-1	6017(27)	6017.225484(16)
2	4	0	6367(30)	6367.765683(17)
2	4	1	6726(33)	6726.356956(18)
2	4	2	7090(36)	7090.515803(19)

Table 8: B -values cancelling $^{85}\text{Rb } 5^2S_{1/2} \rightarrow 6^2P_{3/2} \pi$ transitions.

In table 8, all the B -values obtained are either between 2 and 16 G ie. small values of B , either after 6000 G ie. huge values of B . For the last 4 transitions, the uncertainties are huge, similarly to transitions 1, 10 and 13 of figure 13.

F_g	F_e	m_{F_g}	$B(\text{G})$	$B^*(\text{G})$
3	2	1	4.7610(65)	4.7610264016(37)
3	2	0	4.9572(70)	4.9572750343(38)
3	2	-1	5.1947(76)	5.1947367200(40)
3	2	-2	5.4915(84)	5.4915494036(42)
3	3	-2	20.189(19)	20.189735198(15)
3	3	-1	23.036(20)	23.036018017(18)
3	3	0	26.064(20)	26.064610199(21)
3	3	1	29.313(20)	29.313263093(24)
3	3	2	32.813(20)	32.813410682(27)
2	1	0	46.62(48)	46.624063888(36)
2	1	-1	52.69(48)	52.687400374(41)
2	1	-2	59.84(46)	59.841534398(47)
3	1	0	69.65(42)	69.651160862(54)
3	1	-1	76.78(44)	76.787359782(59)
3	1	-2	84.76(46)	84.761785943(65)
3	2	-3	93.67(48)	93.677445672(70)

Table 9: B -values cancelling $^{85}\text{Rb } 5^2S_{1/2} \rightarrow 6^2P_{3/2} \sigma^+$ transitions.

6. Conclusion and perspectives

In this paper, we dressed an overall view of the theoretical behavior of $5S \rightarrow 6P$ transition cancellations for both Rubidium isotopes. To sum up, all the constants involved are known to around 10^{-10} which is not the case for the ESED. The experimental measurements is envisaged to be done soon at the Institute for Physical Research of Ashtarak, Armenia. To obtain precise results and avoid transition overlapping due to Doppler broadening, sub-Doppler methods have to be used here. This could be achieved using saturated absorption, in which sub-Doppler resolution is attained by forming atomic velocity-selective optical pumping (VSOP) resonances. These VSOPs are accompanied by strong crossover (CO) resonances which complicate the spectra [22]. Another way to obtain sub-Doppler resolution is to use a nano-cell, since Doppler broadening is simply annihilated by the geometry of the cell. Considerably good results have been obtained using nanocells [23, 24] in which the magnetic field can be considered to be uniform due to the cell's thinness. Experimental results will be highly influenced by the experimental

technique that will be used (or developed) to measure the magnetic field. In every table, we showed the B -values computed when taking into account the uncertainty of every parameter, and the B^* -values computed when assuming the ESED to be exact. It is clearly seen that the precision on these values dramatically decreases when the uncertainties on the ESED are taken into account. The measured values could be used to refine uncertainties of all the parameters involved in the problems: ESED, Bohr magneton and even Landé factors. In a reverse way, making an experiment to refine the values of the ESED would also increase the precision of our computations. Moreover, the B -values are determined by analytical formulas meaning they could be used as standard to calibrate magnetometers.

7. Funding Information

A. Aleksanyan thanks the Graduate School EUR EIPHI for the funding CO.17049.PAC.AN.

References

- [1] E. Arimondo, M. Inguscio, P. Violino, Experimental determinations of the hyperfine structure in the alkali atoms, *Rev. Mod. Phys.* 49 (1977) 31–75. URL: <https://link.aps.org/doi/10.1103/RevModPhys.49.31>. doi:10.1103/RevModPhys.49.31.
- [2] C. Pethick, H. Smith, *Bose-Einstein condensation in dilute gases*, Cambridge University Press (2002).
- [3] R. Legaie, C. J. Picken, J. D. Pritchard, Sub-kilohertz excitation lasers for quantum information processing with Rydberg atoms, *J. Opt. Soc. Am. B* 35 (2018) 892–898. URL: <http://josab.osa.org/abstract.cfm?URI=josab-35-4-892>. doi:10.1364/JOSAB.35.000892.
- [4] S. V. Pappu, Information storage using alkali halide crystals, *Contemporary Physics* 26 (1985) 479–497. URL: <https://doi.org/10.1080/00107518508210985>. doi:10.1080/00107518508210985.
- [5] M. Auzinsh, D. Budker, S. Rochester, *Optically Polarized Atoms: Understanding light-atom interactions*, Oxford University Press (2010). Revised paperback Ed. 2014.

- [6] C. So, Zeeman-tunable Modulation Transfer Spectroscopy, Durham theses, Durham University, 2020. URL: <http://etheses.dur.ac.uk/13481/>.
- [7] L. Weller, K. S. Kleinbach, M. A. Zentile, S. Knappe, C. S. Adams, I. G. Hughes, Absolute absorption and dispersion of a rubidium vapour in the hyperfine Paschen-Back regime, *Journal of Physics B: Atomic, Molecular and Optical Physics* 45 (2012) 215005. URL: <https://doi.org/10.1088/0953-4075/45/21/215005>. doi:10.1088/0953-4075/45/21/215005.
- [8] P. Tremblay, A. Michaud, M. Levesque, S. Thériault, M. Breton, J. Beaubien, N. Cyr, Absorption profiles of alkali-metal D lines in the presence of a static magnetic field, *Phys. Rev. A* 42 (1990) 2766–2773. URL: <https://link.aps.org/doi/10.1103/PhysRevA.42.2766>. doi:10.1103/PhysRevA.42.2766.
- [9] A. Sargsyan, G. Hakhumyan, A. Papoyan, D. Sarkisyan, A. Atvars, M. Auzinsh, A novel approach to quantitative spectroscopy of atoms in a magnetic field and applications based on an atomic vapor cell with $L=\lambda$, *Applied Physics Letters* 93 (2008). URL: <https://doi.org/10.1063/1.2960346>.
- [10] K. A. Khanbekyan, E. Mariotti, A. A. Khanbekyan, L. Moi, A. M. Khanbekyan, Sub-doppler spectroscopy of sodium vapor in an ultrathin cell, *Optics and Spectroscopy* 120 (2016) 701–705. URL: <https://link.springer.com/article/10.1134/S0030400X16050143>. doi:10.1134/S0030400X16050143.
- [11] A. Sargsyan, E. Klinger, Y. Pashayan-Leroy, C. Leroy, A. Papoyan, D. Sarkisyan, Selective reflection from Rb vapor in half- and quarter-wave cells: Features and possible applications, *JETP Letters* 104 (2016) 224–230. doi:10.1134/S002136401616013X.
- [12] E. Klinger, A. Sargsyan, A. Tonoyan, G. Hakhumyan, A. Papoyan, C. Leroy, D. Sarkisyan, Magnetic field-induced modification of selection rules for Rb D_2 line monitored by selective reflection from a vapor nanocell, *The European Physical Journal D* 71 (2017) 216. doi:10.1140/epjd/e2017-80291-6.

- [13] E. Klinger, H. Azizbekyan, A. Sargsyan, C. Leroy, D. Sarkisyan, A. Papoyan, Proof of the feasibility of a nanocell-based wide-range optical magnetometer, *Appl. Opt.* 59 (2020) 2231–2237.
- [14] C. Glaser, F. Karlewski, J. Kluge, J. Grimmel, M. Kaiser, A. Günther, H. Hattermann, M. Krutzik, J. Fortágh, Absolute frequency measurement of rubidium $5S-6P$ transitions, *Phys. Rev. A* 102 (2020) 012804. URL: <https://link.aps.org/doi/10.1103/PhysRevA.102.012804>. doi:10.1103/PhysRevA.102.012804.
- [15] D. Steck, Rubidium 85 D line data (2003). URL: <https://steck.us/alkalidata/rubidium85numbers.pdf>, retrieved June, 30th 2020.
- [16] D. Steck, Rubidium 87 D line data (2003). URL: <https://steck.us/alkalidata/rubidium87numbers.pdf>, retrieved June, 30th 2020.
- [17] H. Hakhumyan, Study of optical and magneto-optical processes in Rb atomic vapor layer of nanometric thickness, Ph.D Thesis, Université Bourgogne Franche-Comté, 2012. URL: <https://tel.archives-ouvertes.fr/tel-00764958>.
- [18] E. Tiesinga, P. Mohr, D. Newell, B. Taylor, The 2018 CODATA recommended values of the fundamental physical constants (2020). URL: <http://physics.nist.gov/constants>, retrieved June, 30th 2020.
- [19] A. Aleksanyan, R. Momier, E. Gazazyan, A. Papoyan, C. Leroy, Transition cancellations of ^{87}Rb and ^{85}Rb atoms in a magnetic field setting new standards, *J. Opt. Soc. Am. B.* (2020). In press.
- [20] A. Papoyan, S. Shmavonyan, A. Khanbekyan, K. Khanbekyan, C. Marinelli, E. Mariotti, Magnetic-field-compensation optical vector magnetometer, *Appl. Opt.* 55 (2016) 892–895. URL: <http://ao.osa.org/abstract.cfm?URI=ao-55-4-892>. doi:10.1364/AO.55.000892.
- [21] H. Azizbekyan, S. Shmavonyan, A. Khanbekyan, M. Movsisyan, A. Papoyan, High-speed optical three-axis vector magnetometry based on nonlinear Hanle effect in rubidium vapor, *Optical Engineering* 56 (2017) 1–7. URL: <https://doi.org/10.1117/1.OE.56.7.074104>. doi:10.1117/1.OE.56.7.074104.

- [22] E. Klinger, Selective reflection spectroscopy of alkali vapors confined in nanocells and emerging sensing applications, Ph.D Thesis, Université Bourgogne Franche-Comté, 2019. URL: <https://tel.archives-ouvertes.fr/tel-02317761>.
- [23] A. Sargsyan, G. Hakhumyan, C. Leroy, Y. Pashayan-Leroy, A. Papoyan, D. Sarkisyan, Hyperfine Paschen-Back regime realized in Rb nanocell, *Opt. Lett.* 37 (2012) 1379–1381. URL: <http://ol.osa.org/abstract.cfm?URI=ol-37-8-1379>. doi:10.1364/OL.37.001379.
- [24] G. Hakhumyan, C. Leroy, R. Mirzoyan, Y. Pashayan-Leroy, D. Sarkisyan, Study of “forbidden” atomic transitions on D_2 line using Rb nanocell placed in external magnetic field, *The European Physical Journal D* 66 (2012). Available online at <http://dx.doi.org/10.1140/epjd/e2012-20687-2>.

Graphical Abstract

New standard magnetic field values determined by cancellations of ^{85}Rb and ^{87}Rb atomic vapors $5^2S_{1/2} \rightarrow 6^2P_{1/2, 3/2}$ transitions

Rodolphe MOMIER, Artur ALEKSANYAN, Emil GAZAZYAN, Aram PAPOYAN, Claude LEROY

